Breaking Barriers in Nitrate Electroreduction: Robust Cu-Zn Catalysts for Selective Ammonia Production with Ultra-High Rate in Neutral Medium

Abdelrahman M. Abdelmohsen[1], Lobna A. Abdo[1], Ghada E. Khedr[2], Nageh K. Allam[1, *]

[1]Energy Materials Laboratory, Physics Department, School of Sciences and Engineering, The American University in Cairo, New Cairo 11835, Egypt.

[2]Department of Analysis and Evaluation, Egyptian Petroleum Research Institute, Cairo, 11727, Egypt

* Corresponding Author's email: nageh.allam@aucegypt.edu

Contents

Figure S12. AFM images of the content of Cu and Zn samples. (a) Pure Cu, (b) $Cu_{95}Zn_5$, (c) $Cu_{85}Zn_{15}$, (d) $Cu_{70}Zn_{30}$, (e) $Cu_{50}Zn_{50}$, (f) Pure Zn.

Table S3. Roughness factor (RF) measured/extrapolated from AEM.

Figure S13. Ammonia detection using the indophenol blue method. (a) The UV-Vis adsorption spectra with different ammonia concentrations. (b) The linear standard curve for the calculation of ammonia production.

Figure S14. Shows the Gas Chromatography (GC) profile, where the H_2 peak is detected at a retention time of 5.716 (instrument units).

Figure S15. (a) UV−vis absorption spectroscopy for various concentrations of NO_2^--N. (b) Calibration curve used to estimate the concentrations of NO_2^-N

Figure S16. (a) UV−vis absorption spectroscopy for various concentrations of NO_3^--N. (b) Calibration curve used to estimate the concentrations of NO_3^--N

Figure S17. ECSA measurements of the Cu, $Cu_{95}Zn_5$, and $Cu_{85}Zn_{15}$ samples. (a, b, c), Cyclic voltammetry profiles were obtained on the Cu, $Cu_{95}Zn_5$, and $Cu_{85}Zn_{15}$ catalysts at the sweep rates of 20,30,40, 50, 60, 70, 80, 90, 100, 110, and 120 mV/s, respectively. (d, e, f) The determination of double-layer capacitance for each catalyst.

Figure S18. UV−vis absorption spectroscopy for various samples taken every 10 min in Electrolysis for 2 hours for the $Cu_{85}Zn_{15}$ sample.

Figure S19. (a, b) SEM images of the $Cu_{85}Zn_{15}$ sample after stability test.

Figure S20. XRD for $Cu_{85}Zn_{15}$ (a) before and (b) after stability test.

Figure S21. XPS for $Cu_{85}Zn_{15}$ (a) Zn 2p, (b) Cu 2p.

Figure S22. Control experiment.

- ## SI-3 References

Experimental section

- **Materials and Reagents**

Sodium hydroxide (NaOH, 96%), potassium hydroxide (KOH, ≥85%), and Hydrochloric acid (HCl, 37%) were purchased from Sigma-Aldrich. Potassium nitrate (KNO_3) and potassium chloride (KCl) were purchased from Sigma-Aldrich. Absolute ethanol and acetone were purchased from Merck. Ammonium Persulphate from Qualikems. Ferric nitrate nonahydrate ($FeN_3O_9.9H_2O{\cdot}4H_2O$, ≥98.0%) was purchased from Alfa Aesar. Ammonium chloride (NH_4Cl, ≥98%) was purchased from Fischer. Trisodium citrate, Citric acid ($C_8H_8O_7$, 99.5%), and Salicylic acid ($C_7H_6O_3$, 99%) were purchased from Loba Chemie. Sodium nitroferricyanide ($Na_2[Fe(CN)_5NO]$. $2H_2O$, 99%) was purchased from Alpha Chemika. P-Aminobenzene sulfonamide from Alpha Chemika. N-1-naphthyl ethylene diamine dihydrochloride was purchased from Alpha-Chemika, and sulphamic acid from Fluka, Germany. Sodium hypochlorite (NaOCl, approx. 4%w/v) was purchased from SDDFCL. P Dimethyl Amino Benzaldehyde ($C_9H_{11}NO$, 98%) was purchased from Qualikems. Perchloric acid 70% from Loba Chemie Pvt. Ltd, and lead standard 0.1M Pb^{2+} from ORION.

- **Determination of Ion Concentration.**

The UV-Vis spectrophotometer was used to detect the ion concentration of pre- and post-test electrolytes after diluting to appropriate concentrations to match the range of calibration curves.

Determination of NO_3^-_N

Initially, 1.5 mL of the electrolyte after the electrolysis test for 1h was diluted to 5 mL with water. Subsequently, 0.1 mL of 1 M HCl solution and 0.01 mL of 0.8 wt% sulfamic acid solution were added, allowing the color to grow for 10 minutes. Following this, the absorbance was quantified by UV-Vis spectrophotometry within the wavelength range of 200 nm to 300 nm. The ultimate absorbance of Nitrate-N was calculated using the following equation: $A = A_{220}nm - 2A_{275}nm$. A standard curve was established using a series of standard concentrations of potassium nitrate solutions[1].

Determination of NO_2^-_N

The nitrite concentration was analyzed using the Griess test[2]. Grice's reagent was made by mixing (1 g) of p-aminobenzene sulfonamide, (0.1 g) of N-(1-naphthyl) ethylenediamine dihydrochloride, (50 mL) of deionized water, and (2.94 mL) of phosphoric acid to create a colored solution. The general test method is to mix the diluted solution

electrolyte after 1h of electrolysis with 1 mL of this color reagent, and 2 mL DIW. After placing the mixture under normal environmental conditions without exposure to light for 20 min, to record the UV-vis spectra. The absorbance was measured at a wavelength of 540 nm. Subsequently, the concentration of NO_2^- was calculated according to the concentration dilution times. The standard curve was created using a series of standard concentrations of nitrite solution with a similar testing method.

Determination of NH_3_N

The amount of **ammonia** in the solution was determined by using the indophenol blue method[3, 4]. When completing the electrolysis, (2 mL) of 1M NaOH solution containing salicylic acid (5 wt%) and sodium citrate (5 wt%) were added to 2 mL of the diluted solution electrolyte to match the range of calibration curves. Subsequently, (0.2 mL) nitrosoferricyanide $C_5FeN_6Na_2O$ (1 wt%) and (1 mL) of 0.05 M sodium hypochlorite NaClO were introduced. After color development for 2h, the absorbance was measured at 655 nm. A calibration curve relating concentration to absorbance was established using different volumes of standard ammonium chloride solution.

- **Calculations**
  - **Faradaic efficiency (FE) and yield rate (YR)**

Faradaic efficiency was determined based on the electric charge utilized for ammonia synthesis relative to the total charge transmitted through the electrode, as per the equation **Eq. S1.**

$$\mathbf{FE_{NH3} = (8F \times C_{NH3} \times V) / (M_{NH3} \times Q)}$$

$$\mathbf{FE_{NO2} = (2F \times C_{NO2} \times V) / (M_{NO2} \times Q)}$$

For nitrate electroreduction, the yield was calculated by the **Eq. S2.**

$$\mathbf{Yield_{NH3} = (C_{NH3} \times V) / (t \times A)}$$

$$\mathbf{Yield_{NO2} = (C_{NO2} \times V) / (t \times A)}$$

where **8** and **2** are the number of electrons required to reduce nitrate to ammonia and nitrite, respectively. **F** is the Faraday constant (96485 C/mol); $\mathbf{C_{NH3}}$ and $\mathbf{C_{NO2}}$ are the concentration of ammonia and nitrite in the cathodic compartment, estimated from the calibration curve; **V** is the volume of catholyte (50 mL); $\mathbf{M_{NH3}}$ and $\mathbf{M_{NO2}}$ are the molar mass of NH_3 and NO_2. **Q** is the total charge passed through the cathode; **t** is the time of electrolysis, equal to 60 min is the full reaction time, and **A** is the geometric area of the working electrode, 1 cm^2.

- **NO_3^-_N Conversion**

The conversion rate can be calculated as follows: **Eq. S3**

$$\textbf{Conversion} = \Delta C_{NO3^-} / C_0 \times 100\%$$

Where ΔC_{NO3^-} is the concentration difference of NO_3^- before and after electrolysis, C_0 is the initial concentration of NO_3^-.

- **selectivity of NH_3 and NO_2**

The selectivity of ammonia and nitrite was obtained by **Eq. S4**

$$\textbf{Selectivity} = C / \Delta C_{NO3^-} \times 100\%$$

C is the concentration of ammonia or nitrite.

- **Double-Layer Capacitance (C_{dl}) from CV, Pb -UPD, and EIS**

The electrochemical double-layer capacitance (C_{dl}) of the materials was estimated from the Cyclic voltammetry **(CV)** at different scan rates were performed to determine the electrochemical active surface area (ECSA) in a limited potential range without any faradaic processes (-0.15 to -0.1 V vs. Ag/AgCl). and then the geometric double layer capacitance (C_{dl}) was determined by calculating the current density difference ΔJ = (J anodic – J cathodic)/2 as a linear correlation with the scan rate at a given potential. The ECSA was calculated using the following**: Eq. S5**

$$ECSA = \frac{C_{dI}}{C_s} \times ASA$$

Here, C_{dl} is the specific capacitance of the sample, and **ASA** is the actual surface area of the electrode. C_S is equal to 40 mF/cm^2, representing the standard theoretical capacitance of the complete flat surface of the electrode[5].

The **(Pb-UPD)** was calculated using the following: **Eq. S6**

$$ESCA = \frac{\int_{V1}^{V2} idV}{\theta_{Cu_{poly}}}$$

where *i* indicates the current and *V1–V2* illustrates the potential range of the cathodic monolayer peak of the Pb deposition, as shown by the chemical formula:

$$\mathbf{Cu_{surface} + Pb^{2+} + 2e^{-} \rightleftharpoons Cu_{surface}—Pb}$$

where $\boldsymbol{\theta_{Cu\ (poly)}}$ is the typical monolayer of Pb on Cu(poly) measured at 354 μC/cm2, which was the most dominant surface[6, 7].

Electrochemical impedance spectroscopy (EIS) can be used to determine a double-layer capacitance value can be extrapolated from the Constant Phase Elements (CPE) using **eq. S7**[8, 9].

$$C_{CPE} = [Q(R_e^{-1} + R_{CT}^{-1})^{(\alpha - 1)}]^{\frac{1}{\alpha}}$$

Computational details:

All electronic structure relaxations were performed using the Vienna Ab-initio Simulation Package (VASP 5.4.4) code[10]. The electronic wavefunctions were expanded in plane waves with a cutoff energy of 550 eV[11, 12]. To approximate the core electrons, ultrasoft pseudopotentials were adapted. The Perdew–Burke–Ernzerhof (PBE) exchange correlation functional was used to calculate the adsorption energies. We started with a four-atom unit cell of copper and constructed a 3*3 supercell consists of 36 atoms. Cu_{100}, $Cu_{95}Zn_5$, $Cu_{85}Zn_{15}$ and $Cu_{70}Zn_{30}$ systems were modeled and then (111) surfaces were cleaved. DFT models here represent idealized metallic Cu and Cu–Zn surfaces as an electronic proxy for Zn-induced modification of Cu sites. The periodic images were separated by adding a vacuum layer of 20 Å. A (3 × 3 × 1) Monkhorst–Pack k-point was used to sample the Brillouin zone. An energy convergence of $5*10^{-6}$ eV/atom, and a maximum force of 0.01 eV/Å were applied. We apply the computational hydrogen electrode method to calculate the adsorption free energies. VASPSOL was used to investigate the effect of solvation. For more details, see supporting information (SI).

The equations applied for NO_3^- conversion to NH_3 as the following:

$$* + NO_3^- \rightarrow *NO_3 + e^-$$

$$*NO_3 + 2H^+ + 2e^- \rightarrow *NO_2 + H_2O$$

$$*NO_2 + 2H^+ + 2e^- \rightarrow *NO + H_2O$$

$$*NO + H^+ + e^- \rightarrow *NOH$$

$$*HNO + 2H^+ + 2e^- \rightarrow *NH_2OH$$

$$* NH_2OH + 2H^+ + 2e^- \rightarrow * NH_3 + H_2O$$

$$* NH_3 \rightarrow * NH_3 + *$$

where * represents the surface. Then, the reaction Gibbs free energy change can be calculated by the following equation:

$$\Delta G = \Delta E + \Delta ZPE - T\Delta S$$

where ΔE represents the overall energy difference before and after the intermediate adsorption, and ΔEZPE and ΔS denote the variations in zero-point energy and entropy, respectively. The vibrational frequency computations were utilized to determine the zero-point energy and entropy of free molecules and adsorbents. To circumvent the direct calculation of the energy of charged $NO3^-$, gaseous HNO_3 is employed as a reference in the subsequent steps. The adsorption energy of $NO3^-$ (ΔG^*_{NO3}) can be estimated as

$$\Delta G^* NO_3 = G^* NO_3 - G^* - GHNO_{3(g)} + 0.5GH_{2(g)}$$

where G^*_{NO3}, G^*, $G_{HNO3(g)}$ and G_{H2} represent the Gibbs free energy of adsorbed NO_3^-, HNO_3 and H_2 molecules in the gaseous state, respectively. The HER catalytic activity of catalysts can be assessed by ΔG_H, which is defined as were calculated based on.

$$\Delta E = E_{surf+H} - E_{surf} - {}^1/_2 E(H_2)$$

The Gibbs free energy of Hydrogen is calculated using:

$$\Delta G = \Delta E + \Delta ZPE - T\Delta S$$

ΔZPE denotes the variation in zero-point energy, while ΔS represents the variation in entropy between the adsorbed state and the gas phase. Given that ΔZPE - TΔS ≈ 0.24 eV, it follows that ΔG = ΔE + 0.24 eV.

We investigated the effect of solvation on the adsorption energies of the critical step involving the reduction of NO_2* to NO_2H* using an optimized explicit solvation model implemented in VASPSOL. The analysis showed that solvent interactions caused a negligible change in the calculated limiting potential.

- **Figures and Tables**

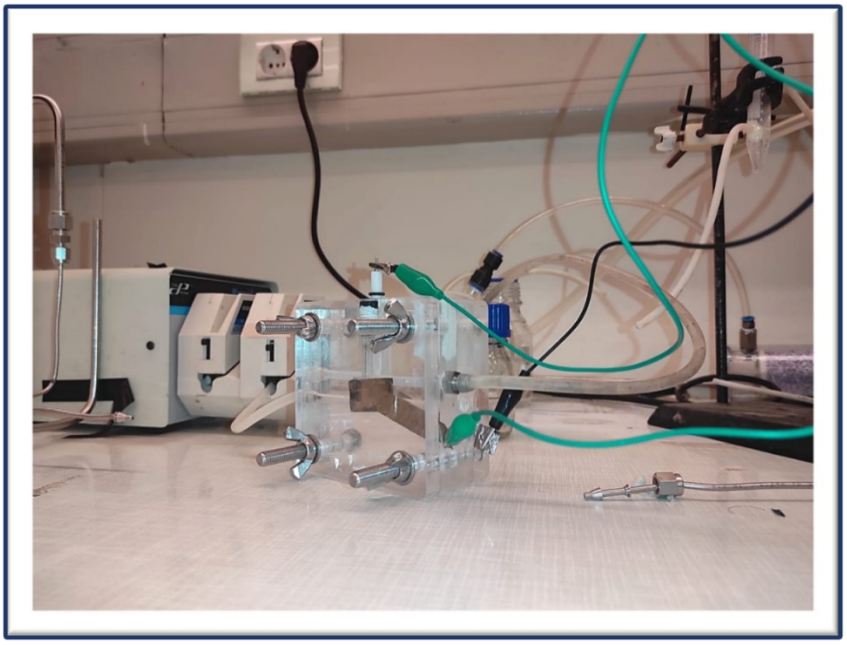

Figure S1. The photo image of the experimental setup for the electrochemical nitrate reduction reaction (NO_3RR).

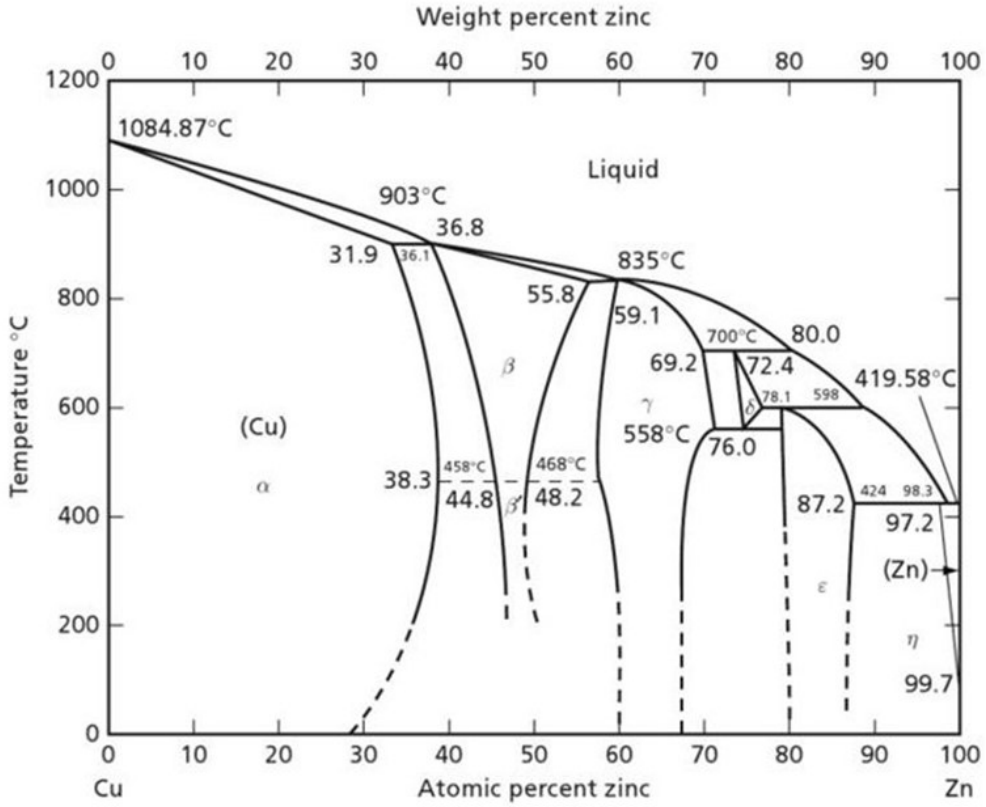

Figure S2. Equilibrium Cu-Zn phase diagram[13].

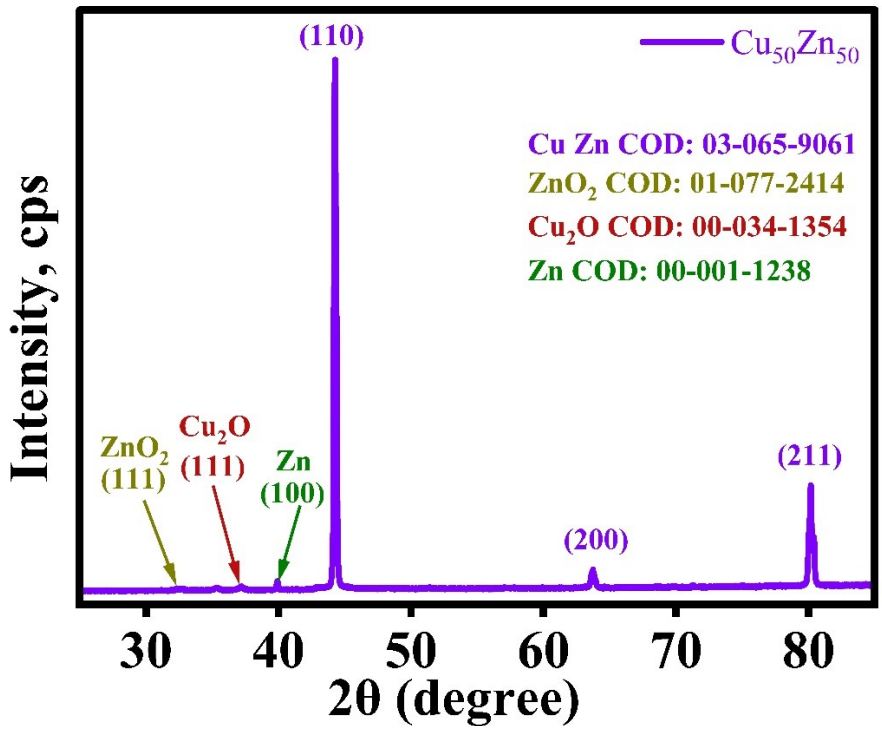

Figure S3. XRD pattern for $Cu_{50}Zn_{50}$ catalyst.

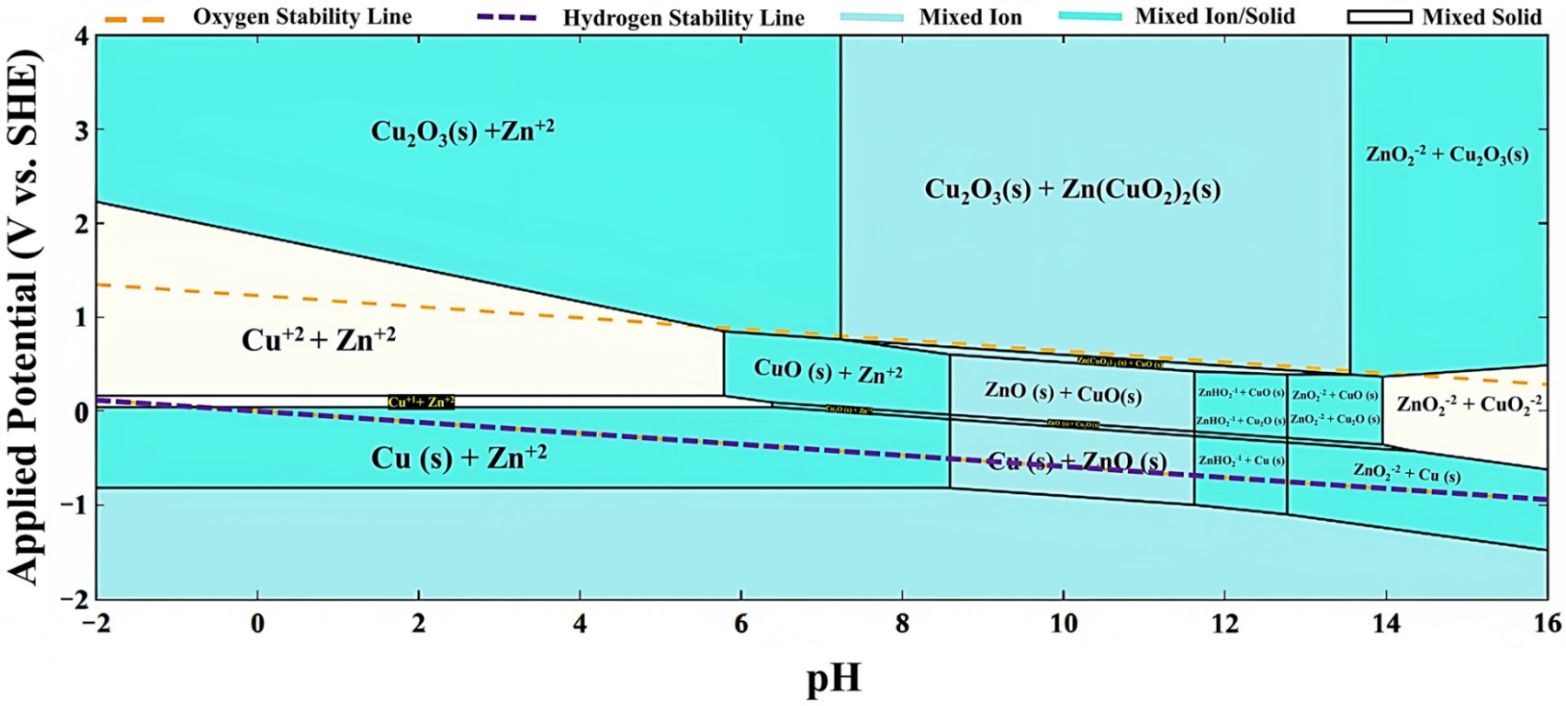

Figure S4. Pourbaix Diagram for **$Cu_{85}Zn_{15}$** sample [14].

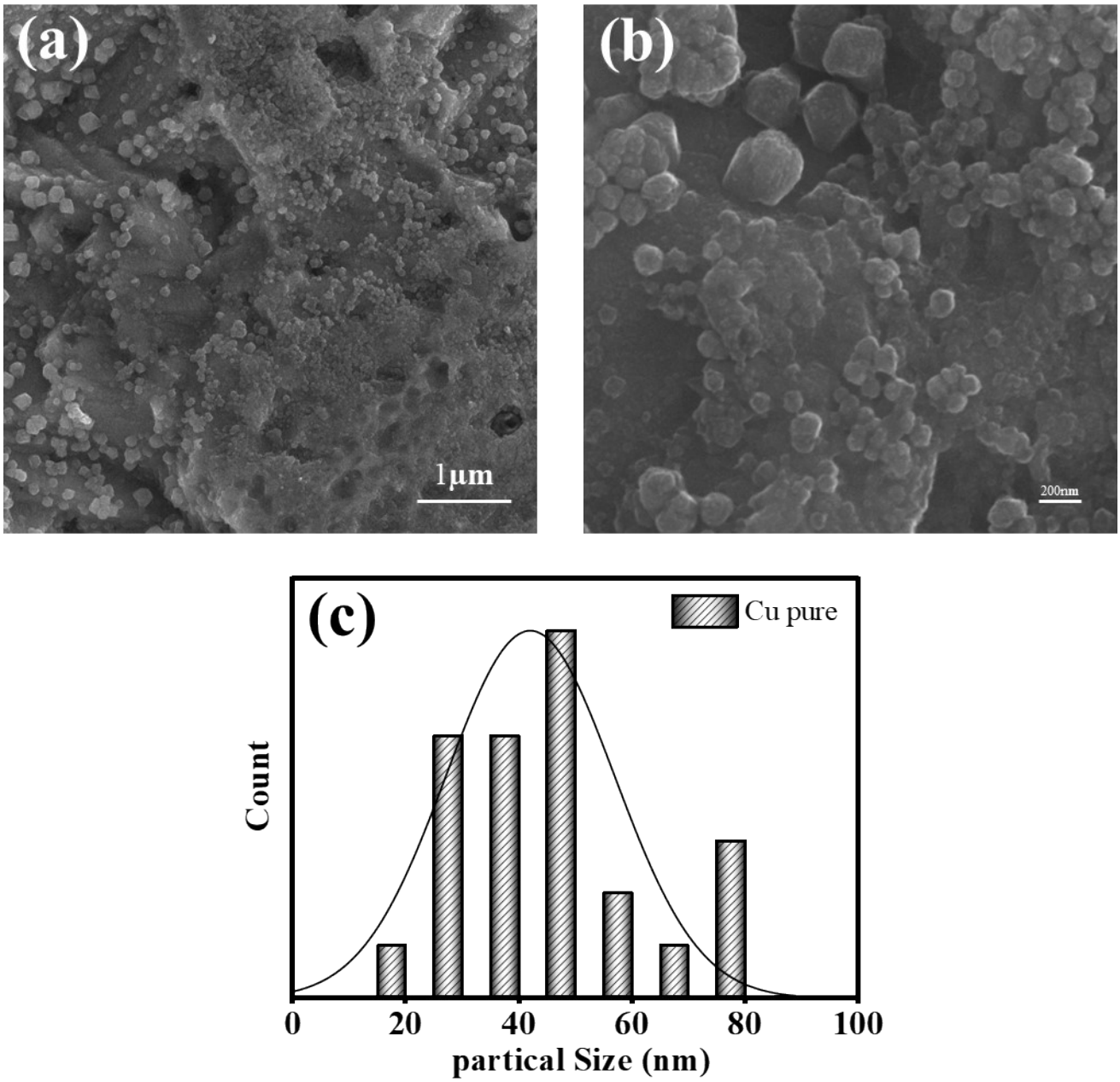

Figure S5. (a, b) SEM images of **Cu-pure** sample, (c) the distribution of the size of nanoparticles.

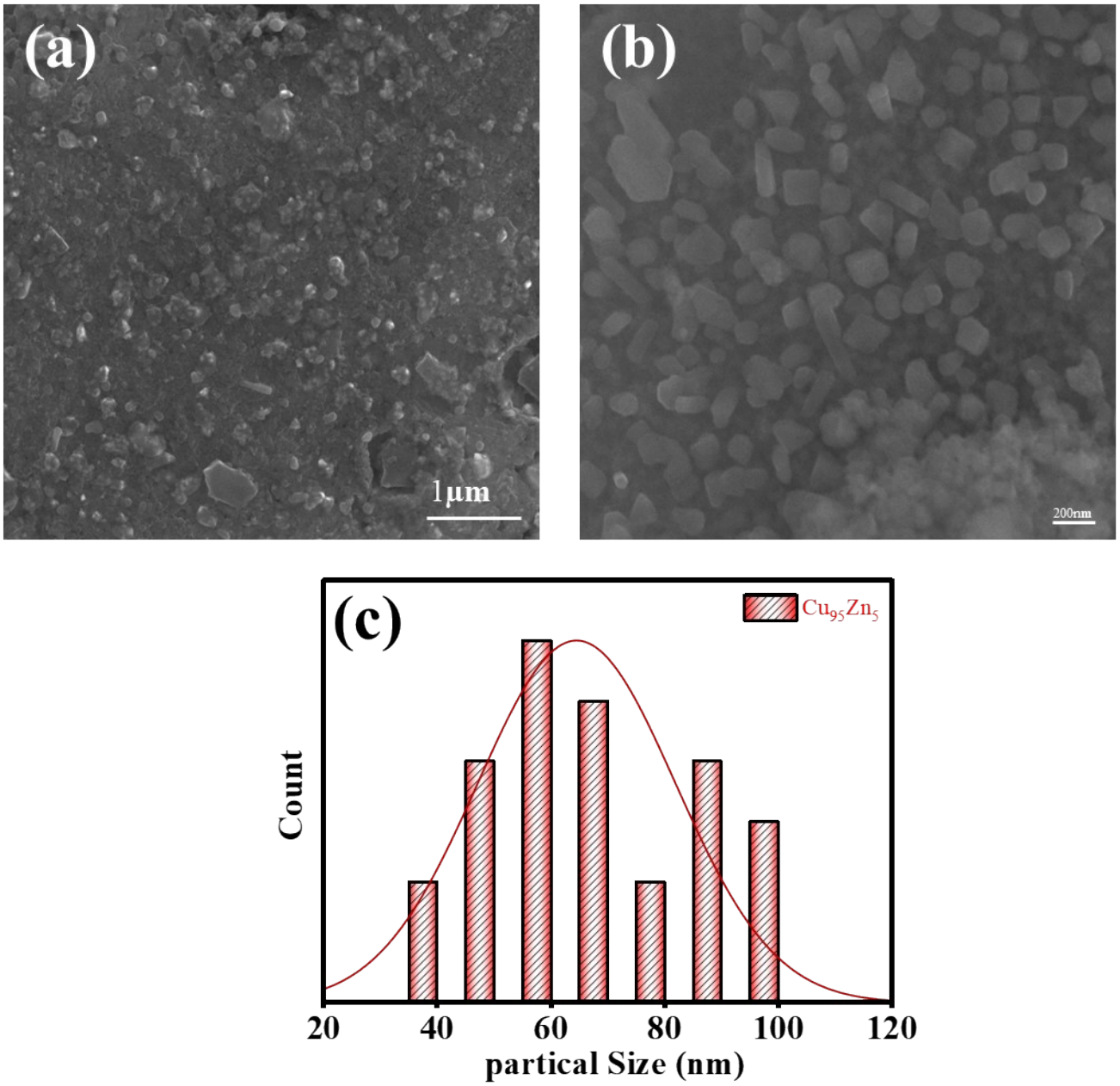

Figure S6. (a, b) SEM images of the **$Cu_{95}Zn_5$** sample, (c) the distribution of the size of nanoparticles.

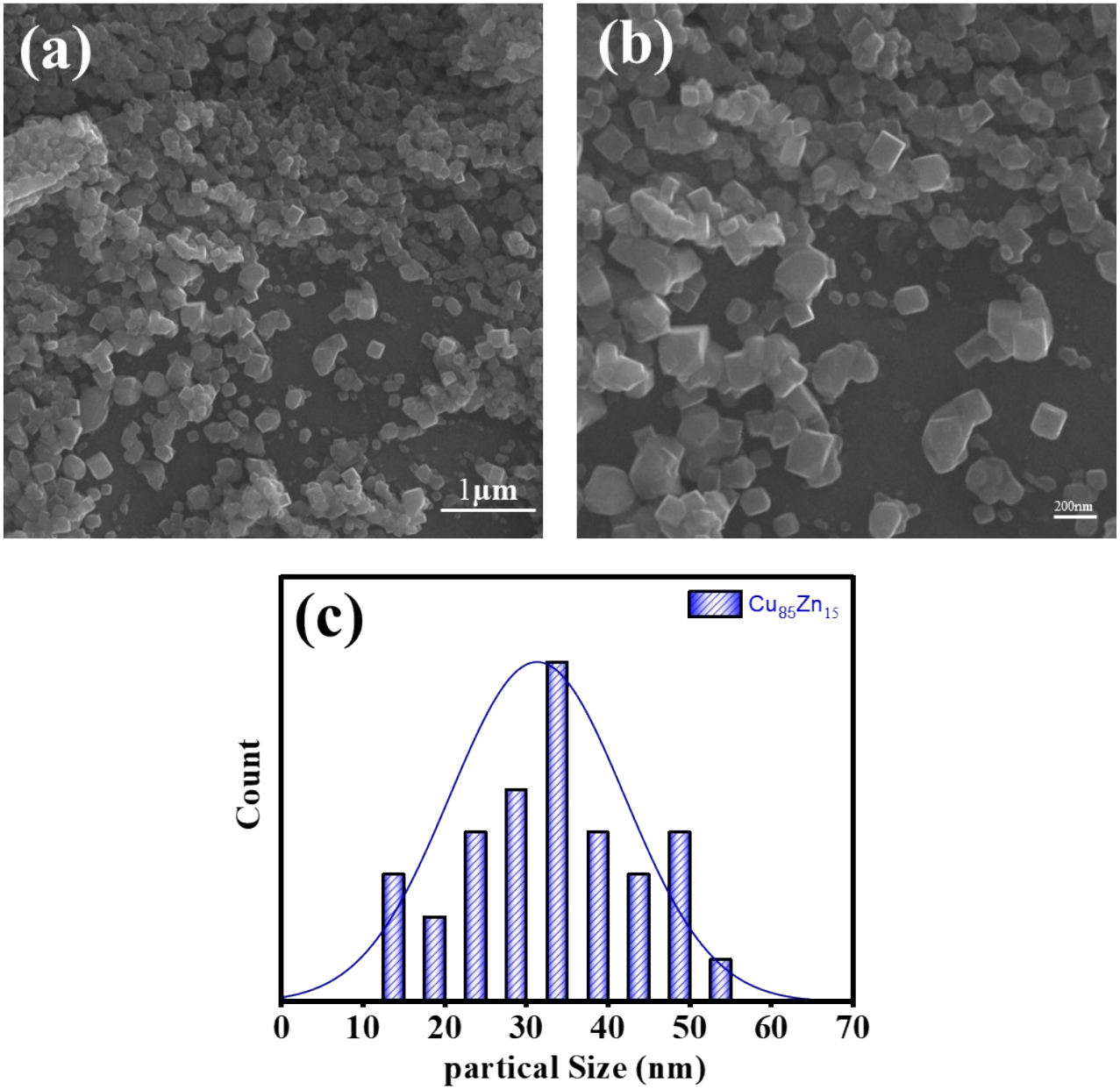

Figure S7. (a, b) SEM images of the $\mathbf{Cu_{85}Zn_{15}}$ sample, (c) the distribution of the size of nanoparticles.

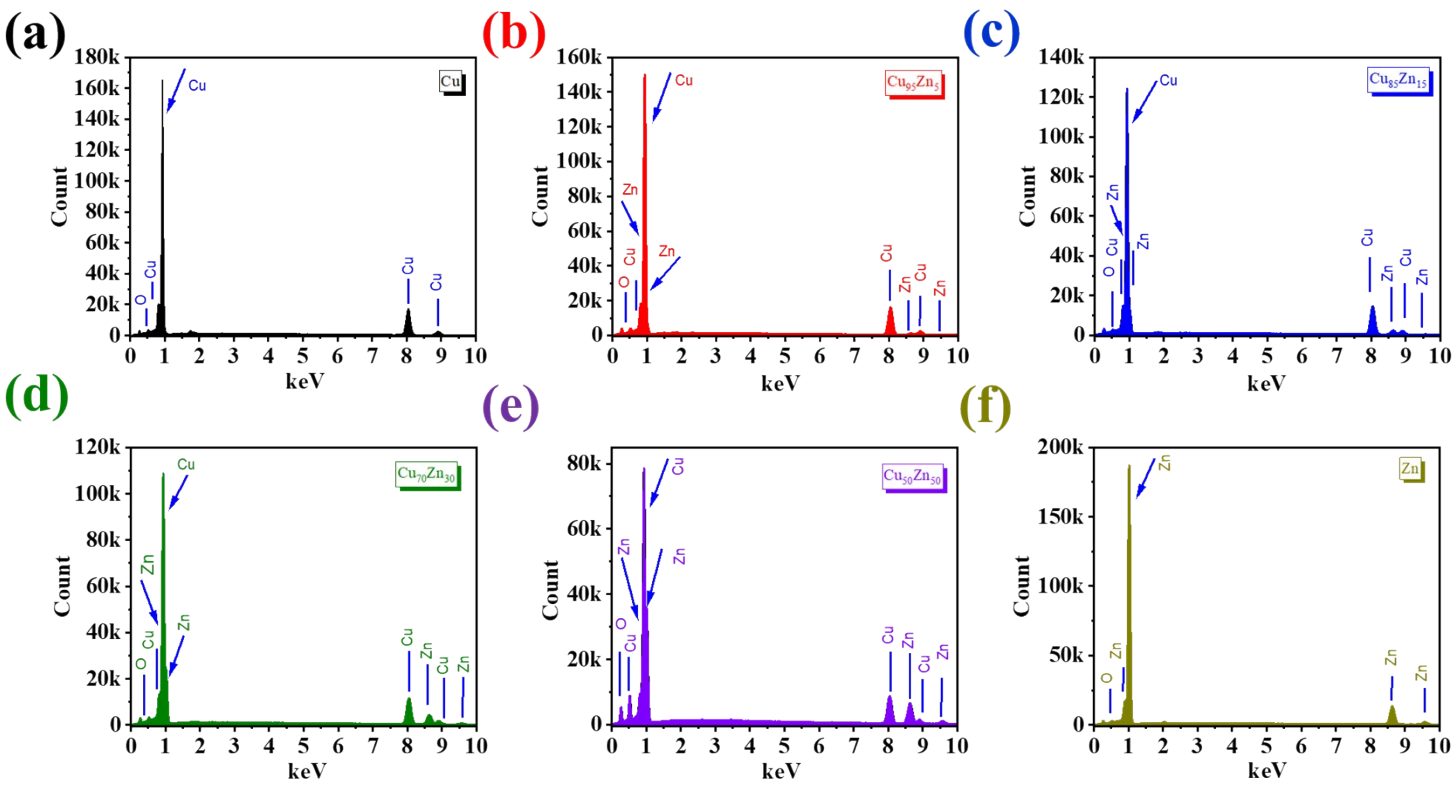

Figure S8. EDX measurements of the content of Cu and Zn for the bare, cleaned, and polished samples. (a) Pure Cu, (b) $Cu_{95}Zn_5$, (c) $Cu_{85}Zn_{15}$, (d) $Cu_{70}Zn_{30}$, (e) $Cu_{50}Zn_{50}$, (f) Pure Zn.

Table S1. Elemental composition of all samples as revealed from the EDX analysis.

Element / Sample	Pure Cu	$Cu_{95}Zn_5$	$Cu_{85}Zn_{15}$	$Cu_{70}Zn_{30}$	$Cu_{50}Zn_{50}$	Pure Zn
	Mass%					
Cu	99.46	93.94	84.43	68.48	51.09	-
Zn	-	5.34	15.31	31.08	48.27	99.62
O	0.54	0.72	0.27	0.45	0.64	0.38

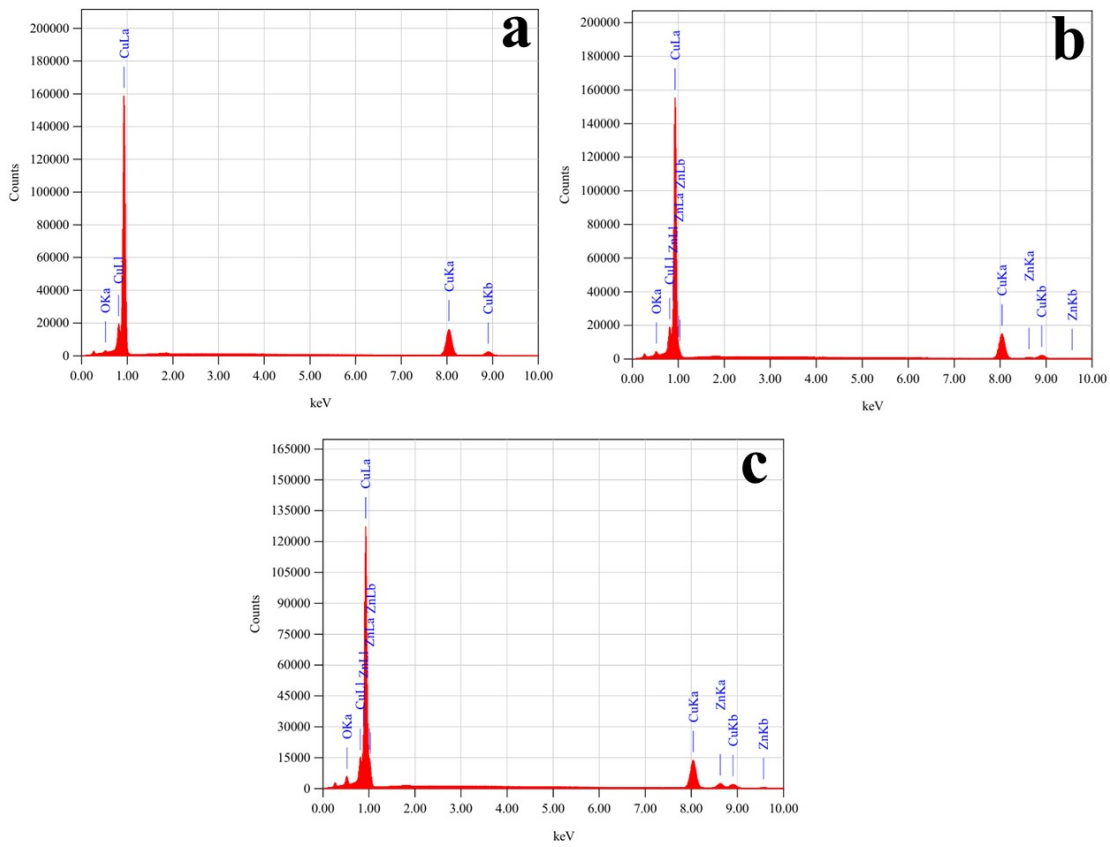

Figure S9. EDX measurements of the content of Cu and Zn for the samples after annealing. (a) **Pure Cu**, (b) **$Cu_{95}Zn_5$**, and (c) **$Cu_{85}Zn_{15}$**

Table S2. Elemental composition of the samples after annealing, as revealed from the EDX analysis

Element / **Sample**	**Pure Cu**	**$Cu_{95}Zn_5$**	**$Cu_{85}Zn_{15}$**
	Mass%		
Cu	**99.5**	**93.8**	**82.38**
Zn	**-**	**5.26**	**15.98**
O	**0.5**	**0.94**	**1.63**

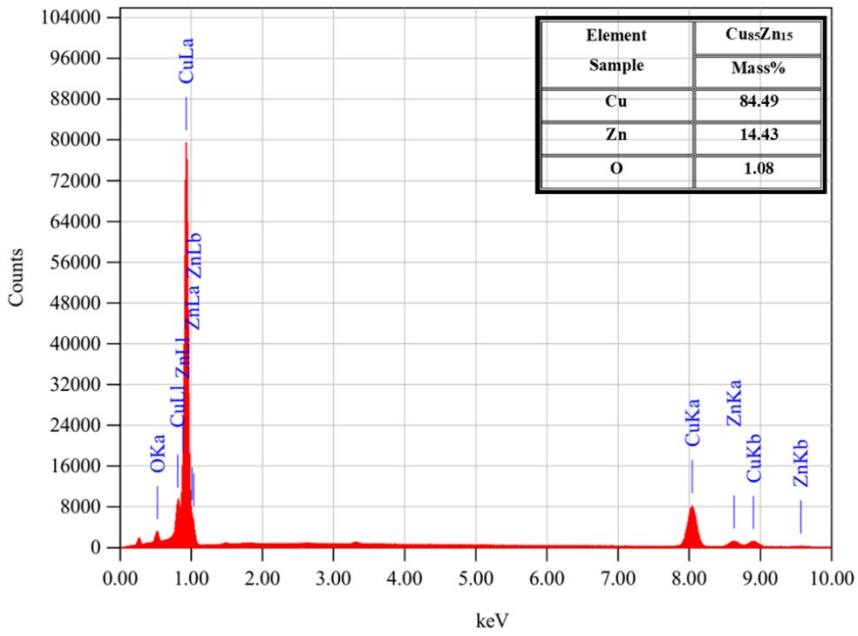

Figure S10. EDX measurements of the sample **$Cu_{85}Zn_{15}$** after electrochemical reaction.

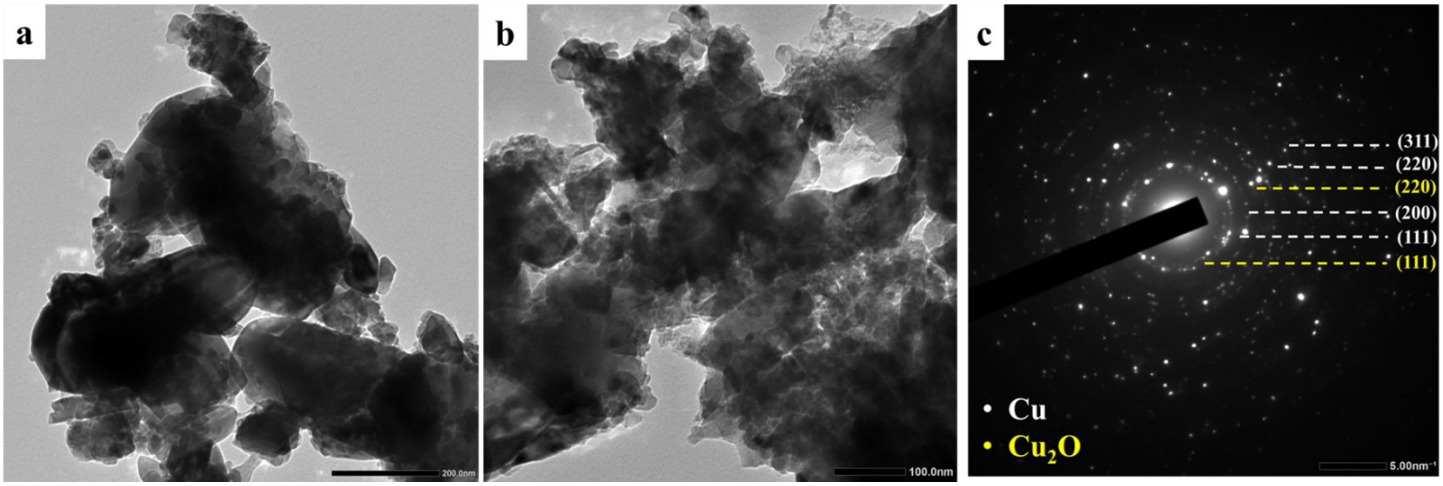

Figure S11. TEM images of the $Cu_{85}Zn_{15}$ sample after the electrochemical reaction: (a, b) TEM, and (c) SAED pattern confirming the coexistence of metallic Cu and Cu_2O phases.

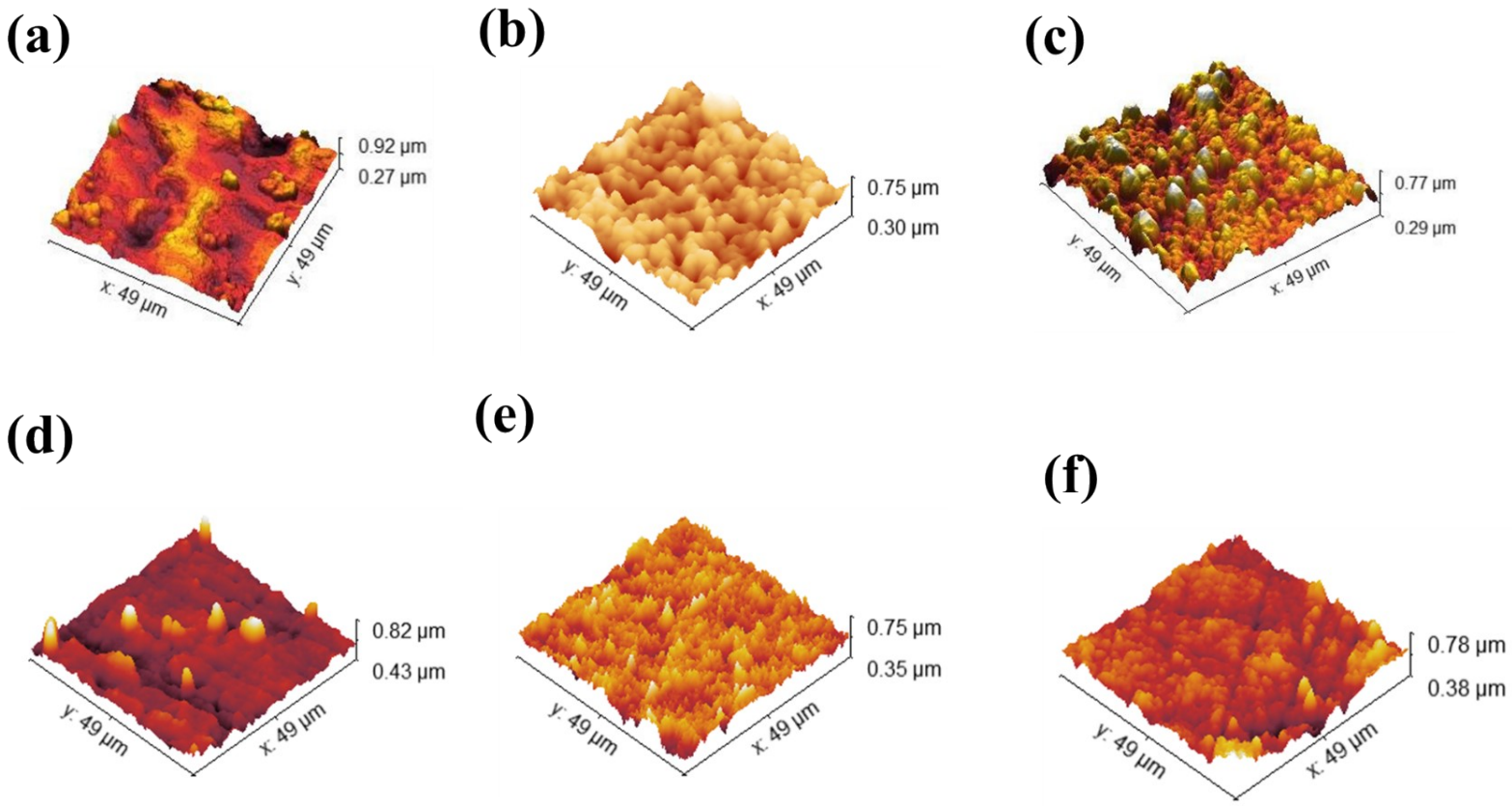

Figure S12. AFM images of the content of Cu and Zn samples. (a) Pure Cu, (b) $Cu_{95}Zn_5$, (c) $Cu_{85}Zn_{15}$, (d) $Cu_{70}Zn_{30}$, (e) $Cu_{50}Zn_{50}$, (f) Pure Zn.

Table S3.

Sample	Cu	$Cu_{95}Zn_5$	$Cu_{85}Zn_{15}$	$Cu_{70}Zn_{30}$	$Cu_{50}Zn_{50}$	Zn
RF from AFM	27.7	20.1	30.2	15.3	17.6	13.9

Roughness factor (RF) measured/extrapolated from AEM.

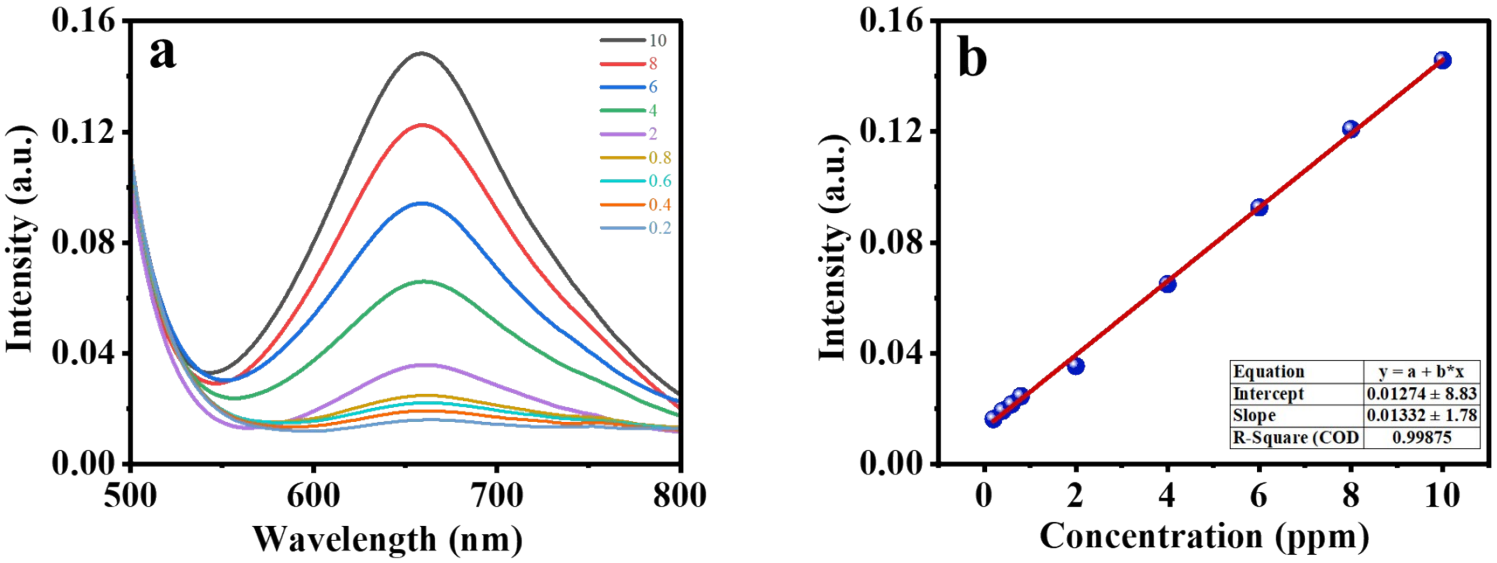

Figure S13. Ammonia detection using the indophenol blue method. (a) The UV-Vis adsorption spectra with different ammonia concentrations. (b) The linear standard curve for the calculation of ammonia production.

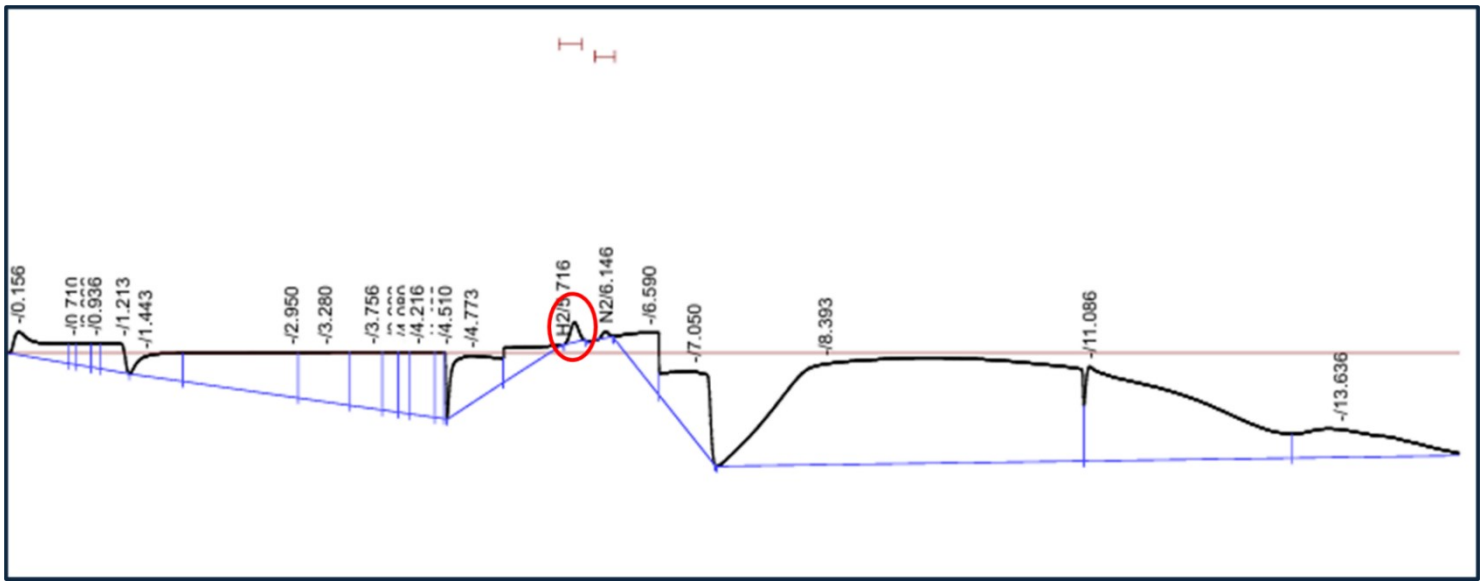

Figure S14. shows the Gas Chromatography (GC) profile, where the H_2 peak is detected at a retention time of 5.716 (instrument units).

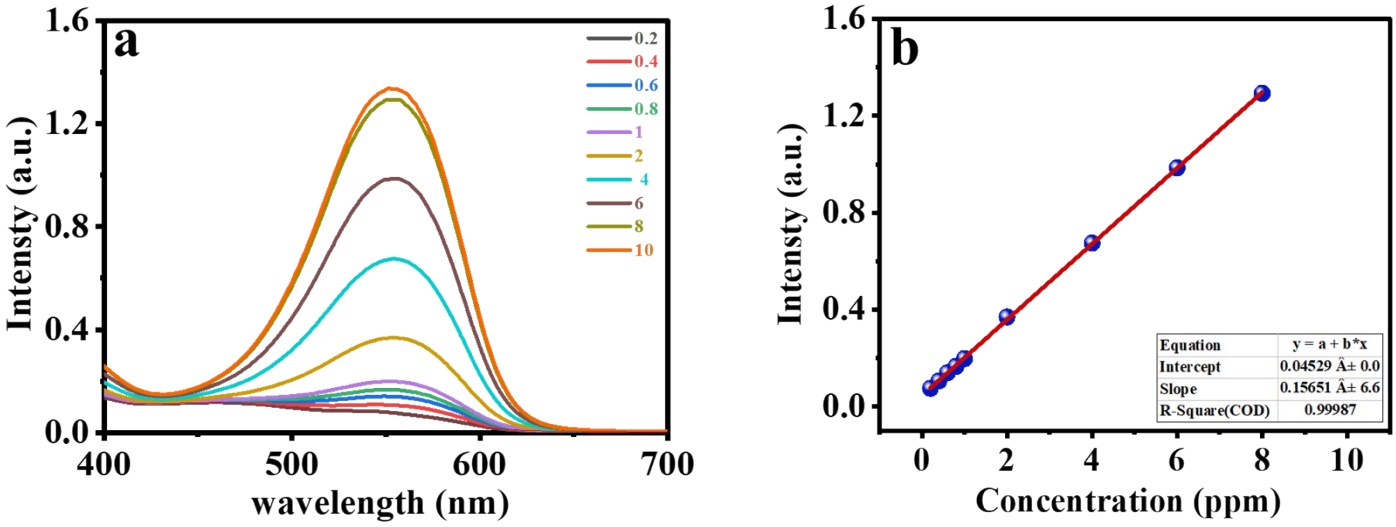

Figure S15. (a) UV−vis absorption spectroscopy for various concentrations of NO_2^--N. (b) Calibration curve used to estimate the concentrations of NO_2^--N

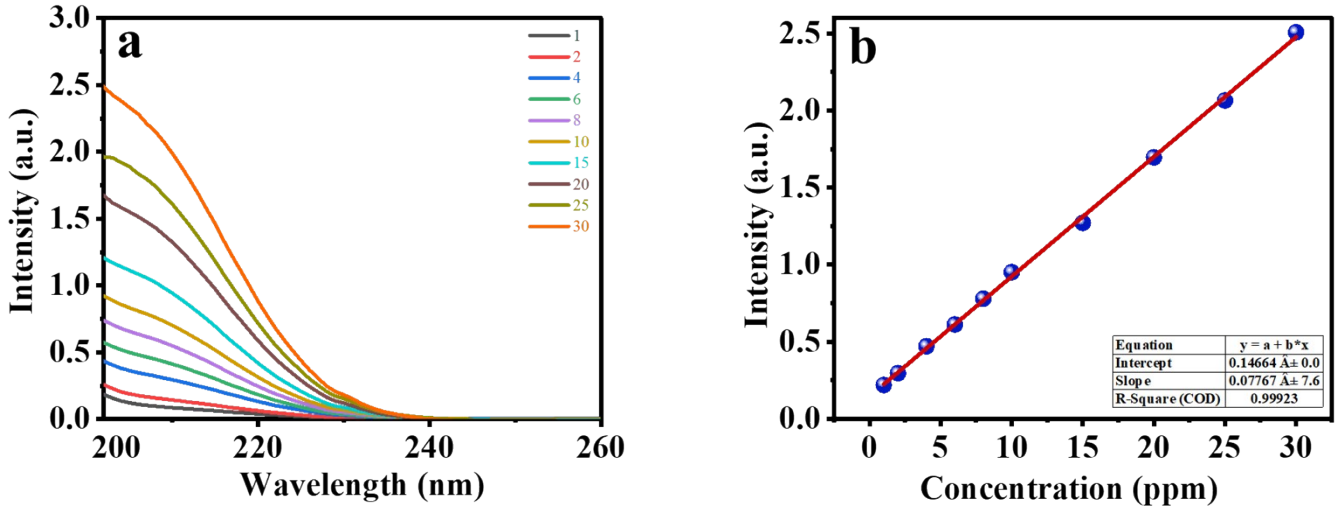

Figure S16. (a) UV−vis absorption spectroscopy for various concentrations of NO_3^--N. (b) Calibration curve used to estimate the concentrations of NO_3^--N

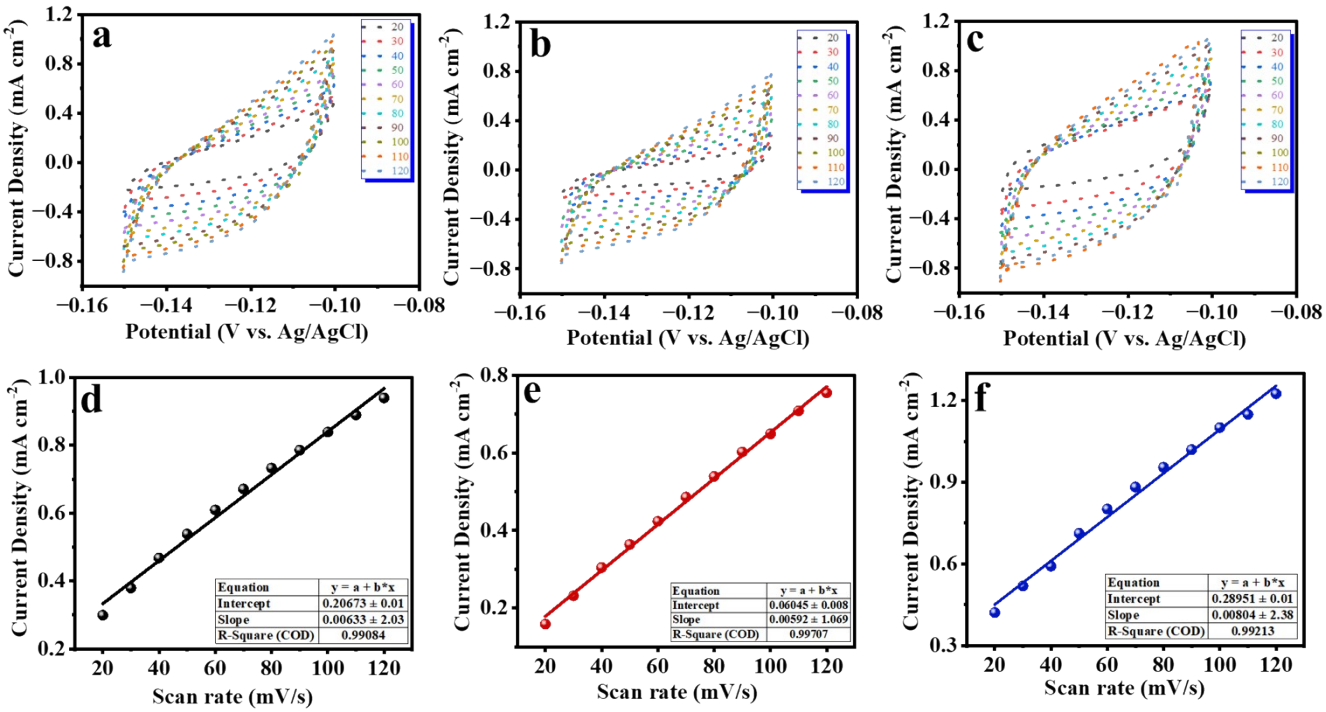

Figure S17. ECSA measurements of the Cu, $Cu_{95}Zn_5$, and $Cu_{85}Zn_{15}$ samples. (a, b, c), Cyclic voltammetry profiles were obtained on the Cu, $Cu_{95}Zn_5$, and $Cu_{85}Zn_{15}$ catalysts at the sweep rates of 20,30,40, 50, 60, 70, 80, 90, 100, 110, and 120 mV/s, respectively. (d, e, f) The determination of double-layer capacitance for each catalyst.

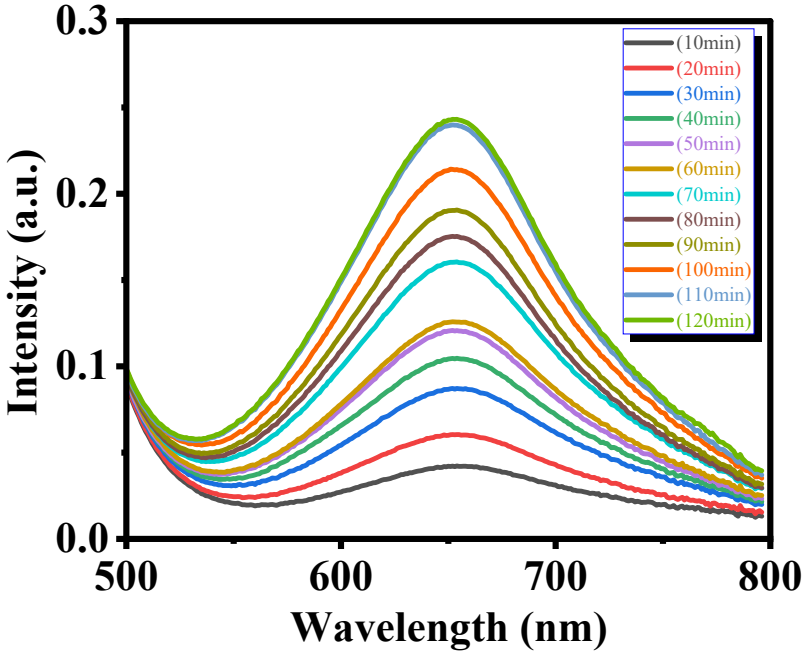

Figure S18. UV−vis absorption spectroscopy for various samples taken every 10 min in Electrolysis for 2 hours for the $Cu_{85}Zn_{15}$ sample.

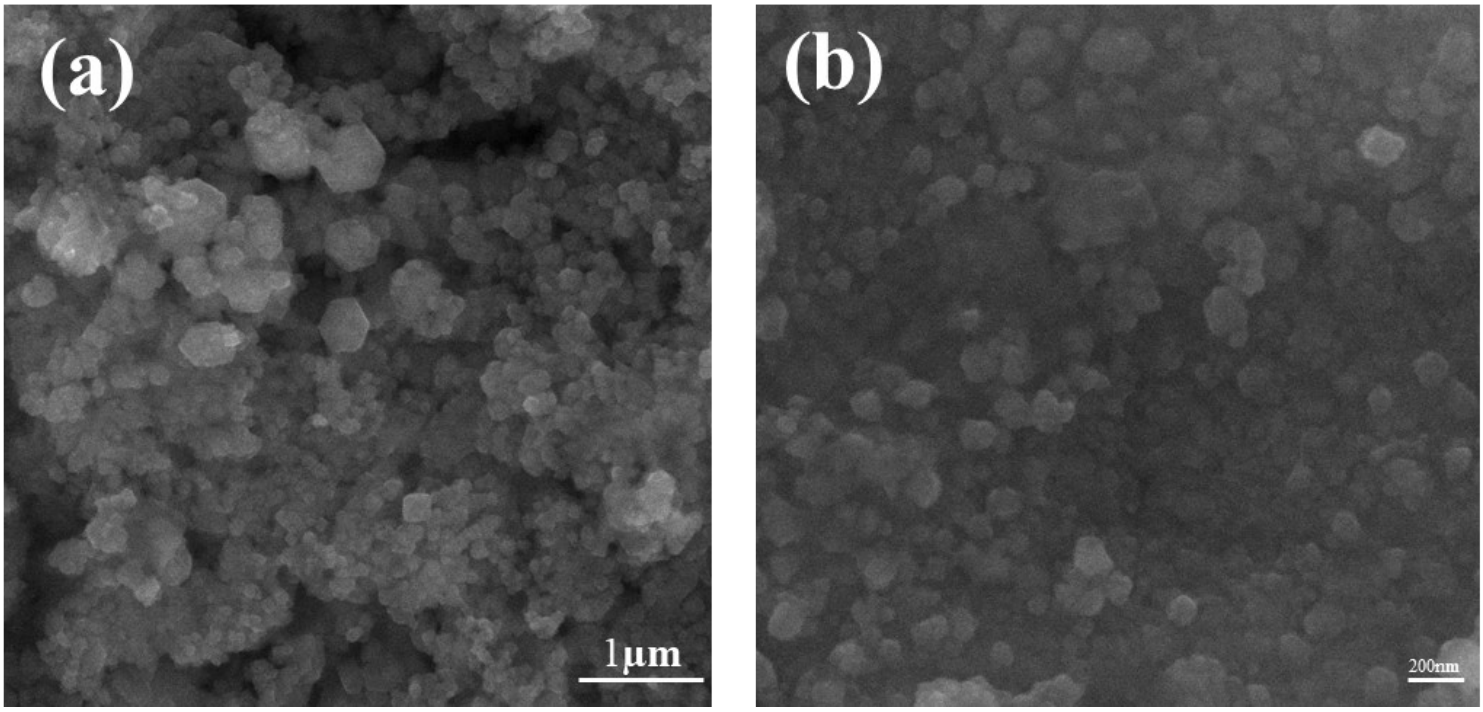

Figure S19. (a, b) SEM images of the $Cu_{85}Zn_{15}$ sample after stability test.

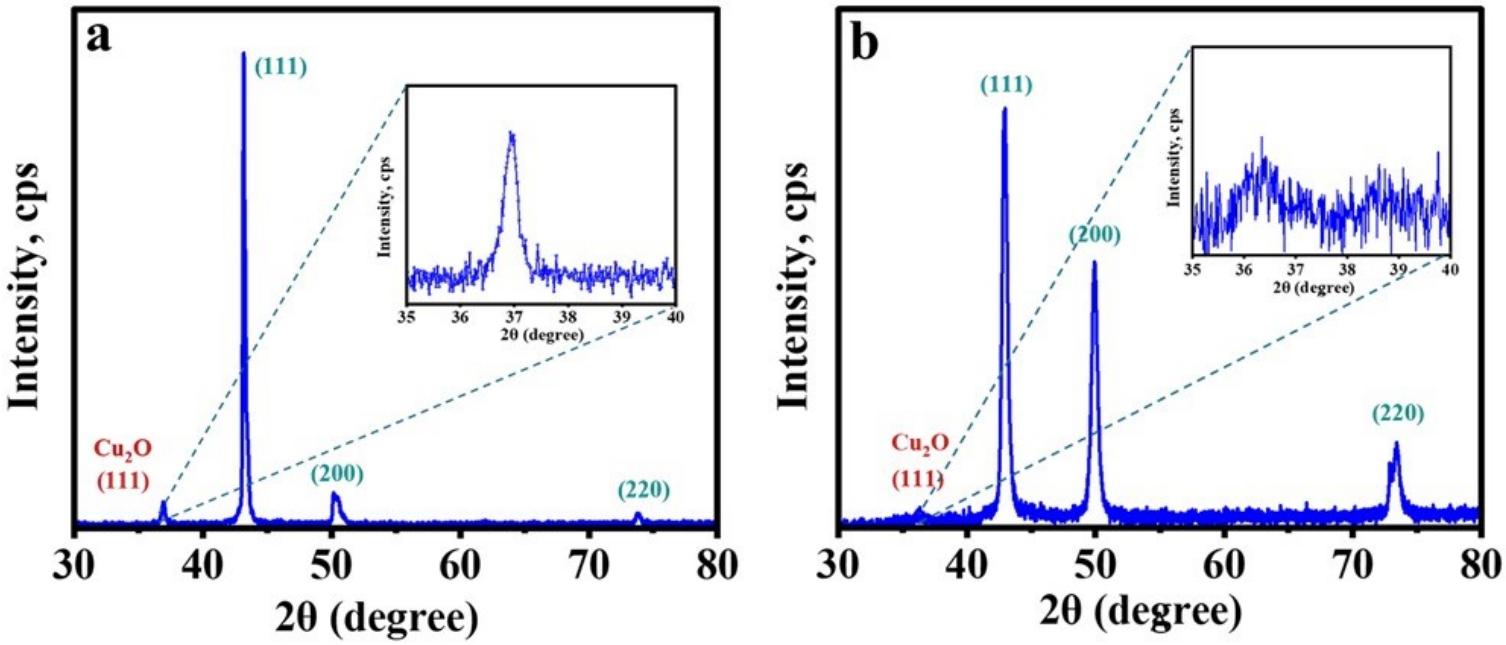

Figure S20. XRD for $Cu_{85}Zn_{15}$ (a) before and (b) after stability test.

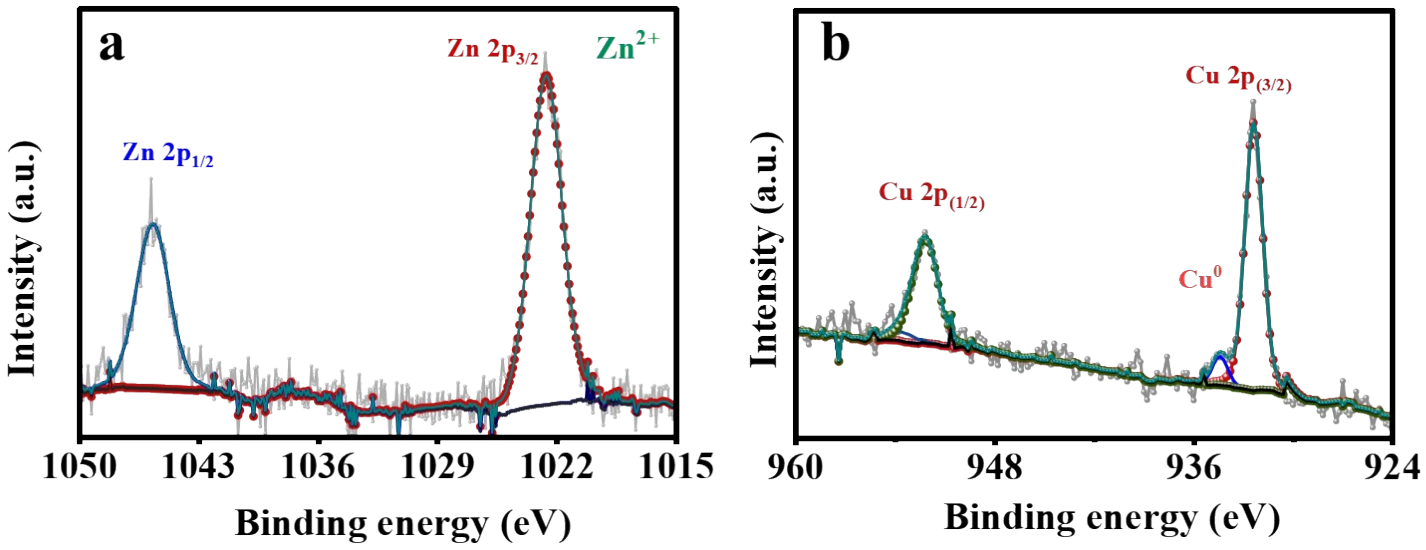

Figure S21. XPS for $Cu_{85}Zn_{15}$ (a) Zn 2p, (b) Cu 2p.

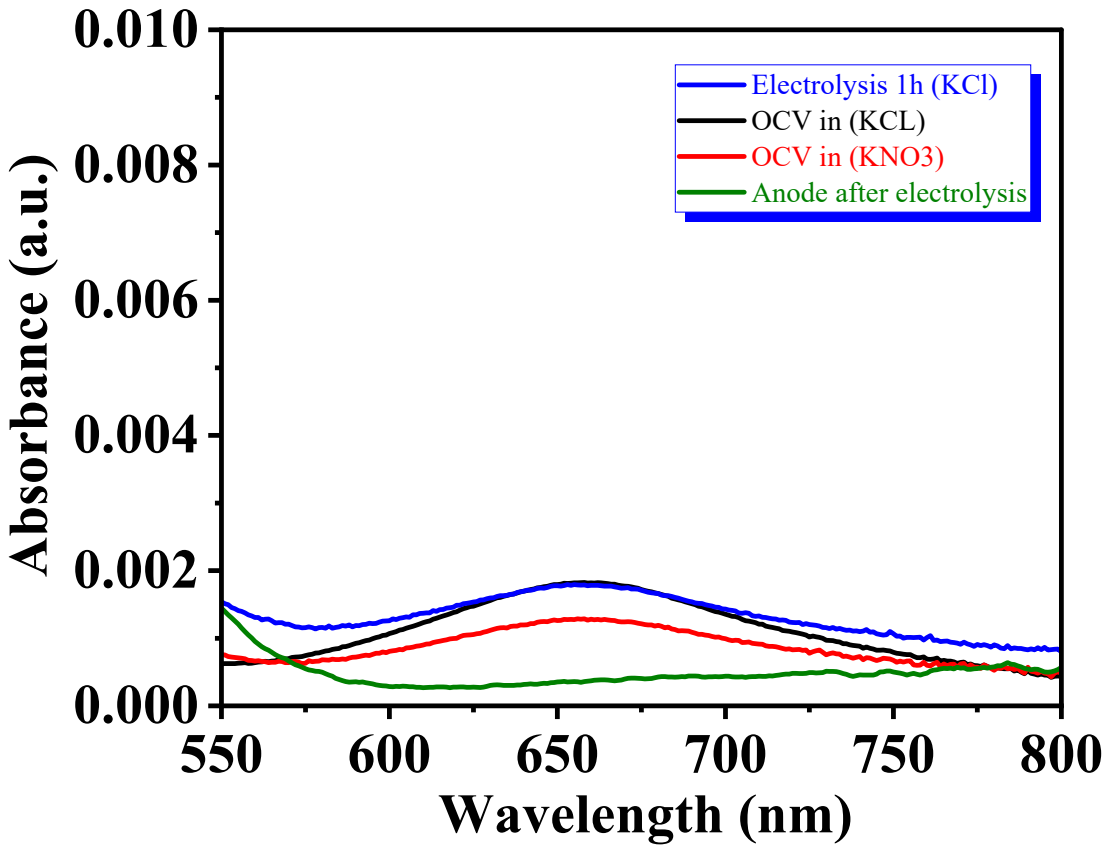

Figure S22. Control experiment

References

1. Y. Xu, K. Ren, T. Ren, M. Wang, M. Liu, Z. Wang, X. Li, L. Wang and H. Wang, *Chemical Communications*, 2021, **57**, 7525-7528.
2. E. Murphy, Y. Liu, I. Matanovic, M. Rüscher, Y. Huang, A. Ly, S. Guo, W. Zang, X. Yan and A. Martini, *Nature communications*, 2023, **14**, 4554.
3. M. Wang, S. Liu, T. Qian, J. Liu, J. Zhou, H. Ji, J. Xiong, J. Zhong and C. Yan, *Nature communications*, 2019, **10**, 341.
4. A. M. Agour, E. Elkersh, G. E. Khedr, H. G. El-Aqapa and N. K. Allam, *ACS Applied Nano Materials*, 2023, **6**, 15980-15989.
5. N. Zhou, Z. Wang, N. Zhang, D. Bao, H. Zhong and X. Zhang, *ACS Catalysis*, 2023, **13**, 7529-7537.
6. L. Yu and R. Akolkar, *Journal of The Electrochemical Society*, 2016, **163**, D247.
7. P. Sebastián-Pascual and M. Escudero-Escribano, *Journal of Electroanalytical Chemistry*, 2021, **896**, 115446.
8. P. Córdoba-Torres, T. J. Mesquita, O. Devos, B. Tribollet, V. Roche and R. P. Nogueira, *Electrochimica Acta*, 2012, **72**, 172-178.
9. A. M. Abdelmohsen, A. M. Agour, I. M. Badawy, G. E. Khedr, Y. Mesbah and N. K. Allam, *Sustainable Energy & Fuels*, 2024, **8**, 3925-3932.
10. G. Kresse and J. Furthmüller, *Physical review B*, 1996, **54**, 11169.
11. G. Kresse and D. Joubert, *Physical review b*, 1999, **59**, 1758.
12. P. E. Blöchl, *Physical review B*, 1994, **50**, 17953.
13. P. Kejzlar, J. Machuta and I. Nová, *Manuf. Technol*, 2017, **17**, 44-48.
14. https://next-gen.materialsproject.org/pourbaix, 14 September 2025.